Sixth International Symposium on Turbulence and Shear Flow Phenomena
Seoul, Korea, 22-24 June 2009

# NUMERICAL SIMULATION OF RIBLET CONTROLLED TRANSITION

**Stephan Klumpp, Matthias Meinke, and Wolfgang Schröder**
Institute of Aerodynamics,
RWTH Aachen University
Wüllnerstraße 5a, 52062 Aachen, Germany
office@aia.rwth-aachen.de

## ABSTRACT

To investigate the impact of riblets aligned in the main flow direction on laminar-turbulent transition large-eddy simulations (LES) of spatially evolving flat plate zero-pressure gradient boundary layer are performed. By superimposed disturbances on the Blasius velocity profile at the inflow boundary natural K-type transition is triggered. A clean surface configuration and two riblet surface configurations are investigated. The two-dimensional Tollmien-Schlichting (TS) waves are found to be amplified by the riblets, whereas three-dimensional disturbances are damped. Secondary flow structures induced by the riblets are found. Overall, transition to turbulence is delayed by the riblets.

## INTRODUCTION

Surface structures, so-called riblets, consisting of tiny grooves aligned with the main flow direction are well known for reducing friction drag in turbulent flow (Bechert et al., 1997). The influence of riblets on the transition from laminar to turbulent flow is, however, not clear, yet. A few experimental investigations, e.g. (Grek et al., 1996; Litvinenko et al., 2006), indicate that there is a delaying effect on the natural transition in zero-pressure gradient boundary layers when the wall is covered by riblets. On the other hand, Ladd et al. (1993) couldn't find any effect of riblets on transition. A reason for this disagreement might be a different spacing in wall units of the used riblets. Natural transition occurs at a low degree of freestream turbulence associated with the development of two-dimensional instability waves known as Tollmien-Schlichting (TS) waves. Their downstream evolution is characterized by a linear amplification, followed by a three-dimensional stage, and finally the turbulent breakdown. Typically, Λ- and hairpin vortices occur in the three-dimensional stage. Grek et al. (1996) concluded from their hot-wire anemometry measurements that the two dimensional waves are amplified by the riblets, whereas the three-dimensional structures are damped. However, no detailed data of the flow close to the wall in the transitional regime is available. A delayed transition by riblets would provide an additional drag reduction capability of riblets.
To gain insight in the damping effect of riblets and to reveal the flow structure in the near-wall region, which is essential to understand the physical mechanism leading to the damping, numerical simulations of spatially evolving natural K-type transition in a flat plate zero-pressure gradient boundary layer above a clean and two riblet walls are performed in the present work. Note that besides the impact of riblets on natural K-type transition also the impact on oblique transition has been investigated. A detailed analysis of these simulations can be found in (Klumpp et al., 2009).

## NUMERICAL METHOD AND VALIDATION

The three-dimensional Navier-Stokes equations for unsteady compressible flow are solved based on a large-eddy simulation (LES) formulation using the MILES (monotone integrated LES) approach (Boris et al., 1992). The discretization of the inviscid terms consists of a mixed centered-upwind AUSM (advective upstream splitting method) scheme (Liou and Steffen Jr., 1993) at second-order accuracy, whereas the viscous terms are discretized second-order accurate using a centered approximation. The temporal integration is done by a second-order explicit 5-stage Runge-Kutta method. A detailed description of the flow solver and a thorough discussion of the quality of its solutions in fully turbulent flow are given, e.g., in (Alkishriwi et al., 2006; Meinke et al., 2002; Renze et al., 2008; Rütten et al., 2005).

The capability to predict natural transition from laminar to turbulent flow is validated by performing a simulation of a temporally evolving transition of a channel flow. To initialize the simulation a parabolic velocity distribution with a superposed two-dimensional Tollmien-Schlichting wave and two oblique waves following the setup of Schlatter et al. (2005) is chosen. At this flow state a formation of Λ-vortices will occur shortly after the flow has been initialized and a K-type transition will take place. Figure 1 shows the Reynolds number $Re_\tau$ based on the local wall friction velocity $u_\tau$ as a function of the dimensionless time compared with the data of Schlatter et al. (2005). Good agreement of the point of transition indicates a proper simulation of the transition mechanisms.

## COMPUTATIONAL SETUP

To simulate flat plate boundary layer transition the computational domain shown in Figure 2 extends $L_x/\delta_i = 440$, $L_y/\delta_i = 14$, and $L_z/\delta_i = 26$ in the streamwise $x$, wall normal $y$, and spanwise direction $z$. Here, $\delta_i$ denotes the displacement thickness at the inlet boundary. For the clean wall case the domain is resolved by $831\times42\times581$ grid points, whereas for the two riblet cases $831\times42\times609$ grid points are used. The riblets rise at $x_s/\delta_i = 47$ for riblet configuration 1 and at $x_s/\delta_i = 160$ for riblet configuration 2. The riblets possess a tip spacing of $s/\delta_i = 0.9$. The riblet geometry was chosen to be similar to that used by Litvinenko et al. (2006), where a transition delay was observed, and to be feasible in a dimension appropriate for technical applications (Hirt and Thome, 2008; Klocke et al., 2007).
Following the setup of Grek *et al.* $Re_{\delta,i} = U_\infty\delta_i/\nu$ is set to 618. The inlet boundary condition is given by a laminar Blasius boundary layer profile with a superposed two-dimensional TS wave with a frequency of $\omega\delta_i/U_\infty = 0.088$ leading to a wavelength of $\lambda_{2d,\alpha} = 27.7\delta_i$ and an amplitude of $\hat{u}_{2d} = 3\times10^{-2}U_\infty$. Furthermore, a three-dimensional oblique wave with the same wavelength in the streamwise di-

rection as the two-dimensional wave, a spanwise wavelength of $\lambda_{3d,\beta} = 26\delta_i$, and an amplitude of $\hat{u}_{3d} = 1 \times 10^{-3} U_\infty$ is superposed. The profiles of the amplitudes of the superposed waves are obtained using a standard Chebyshev collocation method involving the solution of the Orr-Sommerfeld and Squire equations (Schmid and Henningson, 2001). In the spanwise direction periodic boundary conditions are used. A zero pressure-gradient is assumed in the wall-normal direction. On the outflow boundaries the velocity and density gradients are set to zero and the freestream pressure is prescribed. A sponge layer is introduced to damp numerical reflections on the outflow boundaries. In these regions source terms are added to the right-hand side of the governing equations to drive the instantaneous solutions of density and pressure to the desired target solutions.

## RESULTS

In this section first, the results of the numerical simulation of natural K-type transition on the clean surface are presented. Then, the results on the riblet surfaces are given and the impact of the riblets on the Tollmien-Schlichting waves and the three-dimensional structures is analyzed.

### Clean surface configuration

The flow structure on the clean surface is visualized by $\lambda_2$-contours (Jeong and Hussain, 1995) in Figure 3. The typical stages of natural transition as described in the introduction are clearly visible. For a closer investigation the development of the time and spanwise averaged displacement thickness $\delta_1/\delta_i$ and momentum thickness $\delta_2/\delta_i$ are given in Figure 4 together with the empirical laws for laminar and turbulent boundary layers (Ducros et al., 1996). Overall, a good agreement in the laminar and turbulent state is evident and the laminar-turbulent transition is clearly indicated. Also, the development of the spanwise averaged skin-friction coefficient $c_f$ is compared with the empirical laws (Ducros et al., 1996) in Figure 5. The TS waves induced oscillation around the laminar value in the range of $0 \leq x/\delta_i \leq 180$ is followed by a deviation from the laminar value. At $x/\delta_i \approx 280$ the turbulent state is reached. The non-dimensional velocity profile at $x/\delta_i \approx 400$, i.e., slightly upstream of the outflow boundary, is compared with the linear distribution in the viscous sublayer and the log-law distribution in Figure 6. At the same position the Reynolds stresses are compared with the direct numerical simulation data of a fully turbulent boundary layer solution at $Re_{\delta_1} = 1410$ of Spalart (1988), shown in Figures 7 and 8. The Reynolds number based on the local displacement thickness of the current simulation is $Re_{\delta_1} = 927$. Overall, it can be concluded that the agreement with the theoretical data in Figure 6 and the DNS findings in Figures 7 and 8 is convincing and a fully turbulent state near the outflow region of the computational domain is evidenced.

### Riblet surface configuration

The following two sections present firstly, the impact of a riblet surface on the two-dimensional TS waves and secondly, the impact on the three dimensional disturbances.

**Impact on Tollmien-Schlichting waves.** To closer investigate the impact of riblets on TS waves the maximum instantaneous wall-normal velocity in each wall-normal cross section is compared with the clean wall distribution in the range of $0 \leq x/\delta_i \leq 200$ in Figure 9. The maximum wall-normal velocity illustrates the growth of the amplitude of the TS wave. The riblets rise at $x/\delta_i = 47$, which causes the peaks in the maximum velocities. In the range of $50 \leq x/\delta_i \leq 150$ the wall-normal velocity's amplitude on the riblet surface is about 15% higher than on the clean surface. This is illustrated by comparing the peak values in the referred range in Figure 10. The amplification of the TS waves are also evidenced by the development of the spanwise averaged local skin-friction coefficient $c_f$ in Figure 5. The fluctuations on the riblet surface become remarkably stronger than on the clean surface in the same range $50 \leq x/\delta_i \leq 150$. These results of an amplified two-dimensional TS wave agree qualitatively with the findings of Grek et al. (1996) and Luchini and Trombetta (1995). Ehrenstein (1996) shows by a linear stability computation that the laminar channel flow over riblets is more unstable than the parabolic Poisseuille profile with smooth walls. Hence, it seems likely that also at the flat plate boundary layer case the change of the mean velocity profile by the riblets causes the stronger amplification of the TS waves.

**Impact on three-dimensional disturbances.** Since the TS waves at riblet surface configuration 1 are amplified upstream of the point the three-dimensional disturbances start to dominate the flow, a second riblet surface having riblets rising further downstream, i.e., at a streamwise position $x/\delta_i = 160$ where $\Lambda$-structures are already established, is invetsigated. In this way the effects of riblets on the different transition stages can be isolated. The development of the maximum spanwise and wall-normal velocities at riblet surface 2 upstream of the point the riblets rise is nearly identical to the clean surface case. The impact of the riblets on the three-dimensional disturbances is visualized in Figure 5 by the development of the spanwise averaged skin-friction coefficient. Downstream of the point the three-dimensional disturbances starts to dominate the flow, i.e., at $x/\delta_i \approx 160$, the $c_f$-distributions of the riblet surface configurations deviate remarkably from the clean surface. While for the clean wall configuration $c_f$ reaches the turbulent state at $x/\delta_i \approx 300$, the turbulent level is reached not before $x/\delta_i \approx 390$ at the riblet configurations. Note that the likewise development of the skin-friction coefficient at both riblet cases indicates the amplification of the TS waves at riblet surface 1 not to be strong enough to dominate the three-dimensional state of transition. Overall, the delay of the turbulent breakdown by the riblets causes a remarkably skin-friction reduction in this area of up to 40%.

The analysis of the development of the maximum spanwise and wall-normal velocity of the clean surface and riblet configuration 2, illustrated in Figures 11 and 12, gives further insight. In the range of $270 \leq x/\delta_i \leq 330$, where also $c_f$ differs the most, both velocity components at the riblet configuration are approximately 40% smaller compared to the clean wall case. This damping is caused by secondary flow structures induced by the riblets. Figure 13 visualizes the flow structure above the riblet surface by streamlines, where one leg of a hairpin vortex is represented by the large vortex. Besides the expected wave-like overflowing of the riblet tips some recirculation zones are observed resulting in high energy dissipation. The damped strength of the three-dimensional structures causes a damped transport of low-speed fluid from the wall to the outer region of the boundary layer such that the turbulent breakdown into a turbulent spot is delayed (Grek et al., 1996).

## SUMMARY

A set of numerical simulations of spatially evolving zero-pressure gradient boundary layer flow undergoing natural K-type transition from a laminar to a fully turbulent state have been performed. While the two-dimensional TS waves are amplified by streamwisely aligned riblets three-dimensional structures, such as Λ- or hairpin vortices, are damped by the riblets. The damped three-dimensional disturbances lead to a reduced transport of low-speed fluid from the wall near region into the outer regions of the boundary layer, which delays the breakdown to turbulence. Overall, the riblets cause a delay of transition, which clearly reduces the total drag despite the relatively small area affected by this effect.

## ACKNOWLEDGMENTS

The authors gratefully acknowledge the financial support of the joint cooperative project "RibletSkin" by the Volkswagen Foundation, Hannover, Germany.

## REFERENCES

Alkishriwi, N., Meinke, M., and Schröder, W. 2006. A large-eddy simulation method for low mach number flows using preconditioning and multigrid. *Comp. Fluids*, Vol. 35, no. 10, pp. 1126–1136.

Bechert, D. W., Bruse, M., Hage, W., van der Hoeven, J. G. T., and Hoppe, G. May 1997. Experiments on drag-reducing surfaces and their optimization with an adjustable geometry. *J. Fluid Mech.*, Vol. 338, pp. 59–87.

Boris, J., Grinstein, F., Oran, E., and Kolbe, R. 1992. New insights into large eddy simulation. *Fluid Dyn. Research*, Vol. 10, pp. 199–228.

Ducros, F., Comte, P., and Lesieur, M. 1996. Large-eddy simulation of transition to turbulence in a boundary layer developing spatially over a flat plate. *J. Fluid Mech.*, Vol. 326, pp. 1–36.

Ehrenstein, U. Nov. 1996. On the linear stability of channel flow over riblets. *Phys. Fluids*, Vol. 8, pp. 3194–3196.

Grek, G. R., Kozlov, V.V., and Titarenko, S.V. 1996. An experimental study of the influence of riblets on transition. *J. Fluid Mech.*, Vol. 315, pp. 31–149.

Hirt, G. and Thome, M. 2008. Rolling of functional metallic surface structures. *CIRP Annals - Manufacturing Technology*, Vol. 57, no. 1, pp. 317–320.

Jeong, J. and Hussain, F. 1995. On the identification of a vortex. *J. Fluid Mech.*, Vol. 285, pp. 69–94.

Klocke, F., Feldhaus, B., Hirt, G., Klumpp, S., and Schröder, W. 2007. Development of two innovative rolling processes for the production of defined riblet structures in consideration of common fluid dynamic requirements. In *2nd ICNFT, Proc. of the 2nd.International Conference on New Forming Technology, Sept. 20-21, Bremen, Germany*, pp. 185–194.

Klumpp, S., Meinke, M., and Schröder, W. 2009. Numerical simulation of riblet controlled spatial transition in a zero-pressure gradient boundary layer. *submitted to Flow, Turbulence and Combustion.*

Ladd, D. M., Rohr, J. J., Reidy, L. W., and Hendricks, E. W. 1993. The effect of riblets on laminar to turbulent transition. *Exp. in Fluids*, Vol. 14, pp. 1–2.

Liou, M. S. and Steffen Jr., C. J. 1993. A New Flux Splitting Scheme. *J. Comput. Phys.*, Vol. 107, pp. 23–39.

Litvinenko, Y. A., Chernoray, V. G., Kozlov, V. V., Loefdahl, L., Grek, G. R., and Chun, H. H. Mar. 2006. The influence of riblets on the development of a Λ structure and its transformation into a turbulent spot. *Physics - Doklady*, Vol. 51, pp. 144–147.

Luchini, P. and Trombetta, G. Jun. 1995. Effects of Riblets upon Flow Stability. *Applied Scientific Research*, Vol. 54, pp. 313–321.

Meinke, M., Schröder, W., Krause, E., and Rister, Th. 2002. A comparison of second- and sixth-order methods for large-eddy simulations. *Comp. Fluids*, Vol. 31, pp. 695–718.

Renze, P., Schröder, W., and Meinke, M. 2008. Large-eddy simulation of film cooling at density gradients. *Int. J. Heat Fluid Flow*, Vol. 29, pp. 18–34.

Rütten, F., Meinke, M., and Schröder, W. 2005. Large-eddy simulations of frequency oscillation of the dean vorticies in turbulent pipe bend flows. *Phys. Fluids*, Vol. 17, pp. 035107–1–035107–11.

Schlatter, P., Stolz, S., and Kleiser, L. 2005. Computational simulation of transitional and turbulent shear flow. In *Progress in Turbulence, Proc. ITI Conference on Turbulence,*.

Schmid, P. J. and Henningson, D. S. 2001. *Stability and transition in shear flows*. Springer Verlag, New York.

Spalart, P. R. 1988. Direct Simulation of a Turbulent Boundary Layer up to $R_\theta = 1410$. *J. Fluid Mech.*, Vol. 187, pp. 61–98.

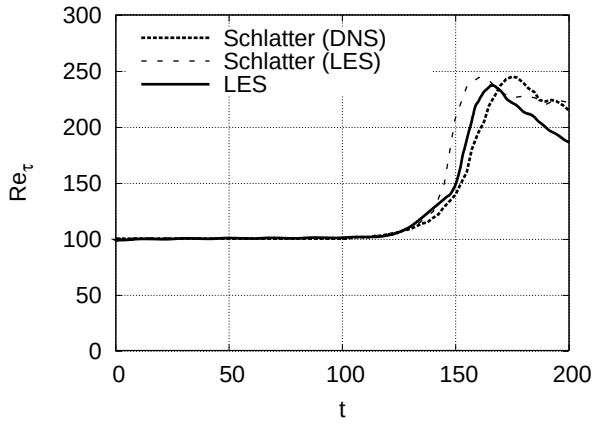


Figure 1: *Friction velocity based Reynolds number $Re_\tau$ vs time.*

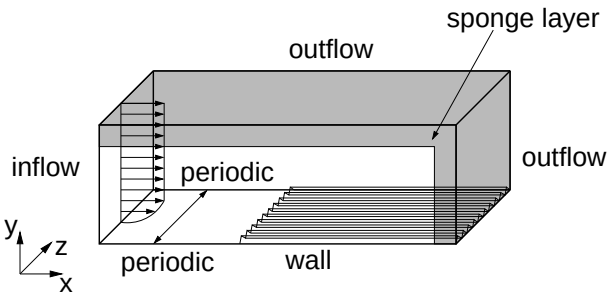


Figure 2: *Computational domain.*

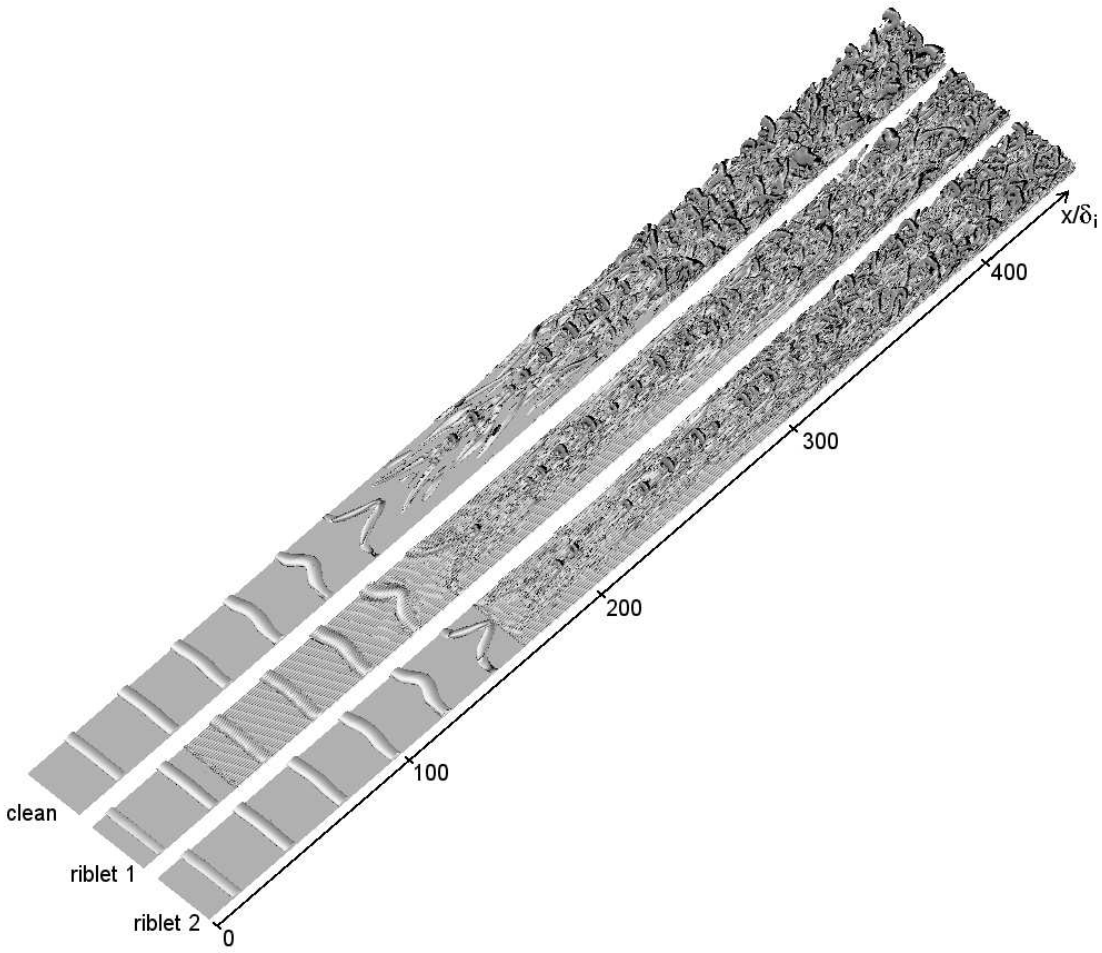


Figure 3: *$\lambda_2$-contours for the clean and the riblet configurations.*

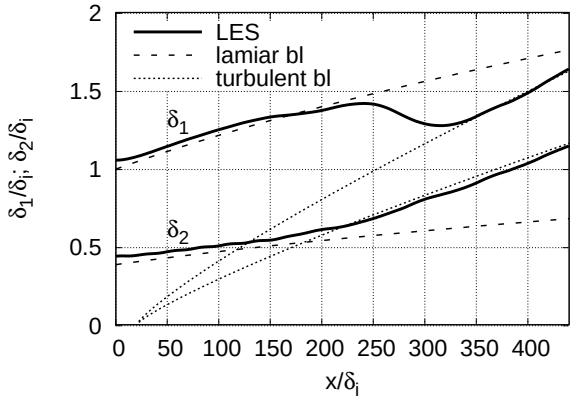


Figure 4: *Displacement thickness $\delta_1$ and momentum thickness $\delta_2$ for the clean wall case.*

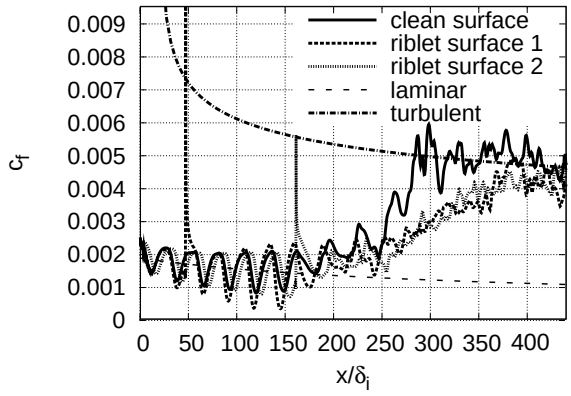


Figure 5: *Local skin-friction coefficient $c_f$ for the clean and the riblet cases.*

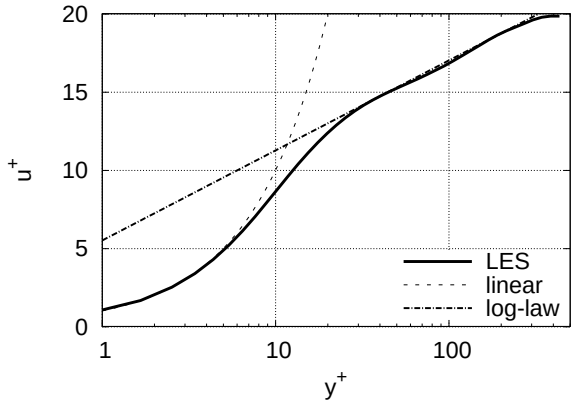


Figure 6: *Velocity profile at $x/\delta_i = 400$ at the clean surface case.*

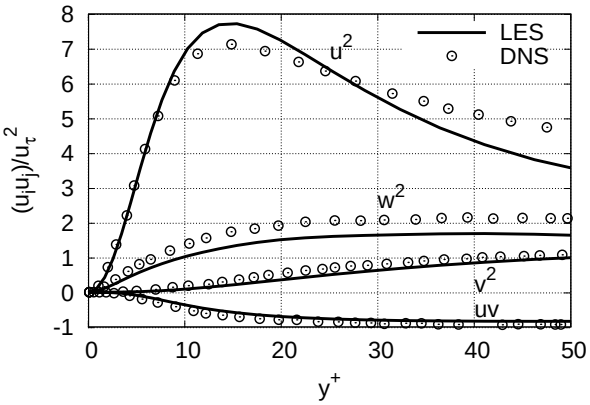


Figure 7: *Reynolds stresses of the clean wall surface problem at $x/\delta_i = 400$ in inner coordinates; solid line: current LES, symbols: DNS from (Spalart, 1988).*

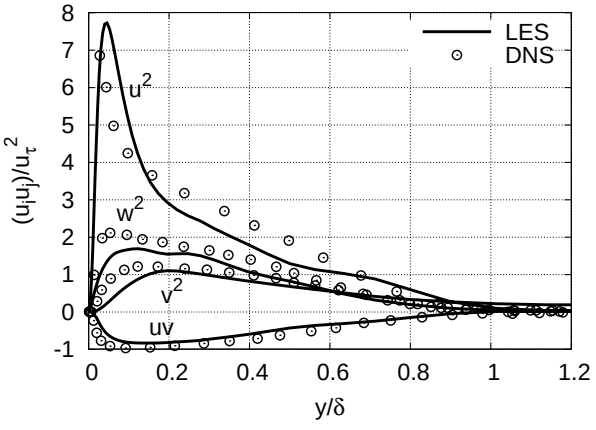


Figure 8: *Reynolds stresses of the clean wall surface problem at $x/\delta_i = 400$ in outer coordinates; solid line: current LES, symbols: DNS from (Spalart, 1988).*

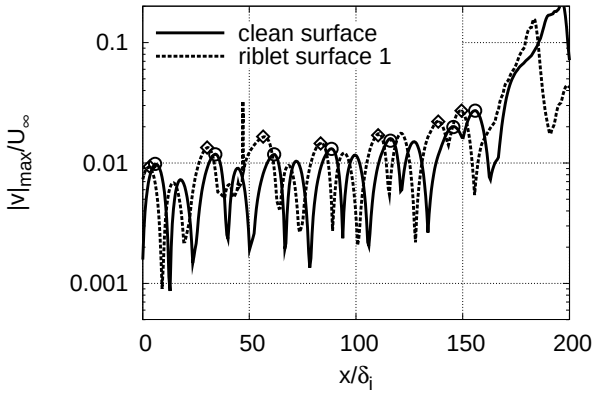


Figure 9: *Maximum wall-normal velocity $|v|_{max}$ vs $x/\delta_i$.*

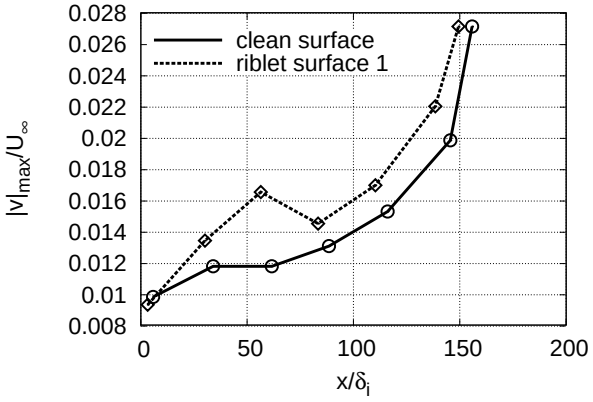


Figure 10: *Comparison of the local maxima in the streamwise direction of the wall-normal velocity illustrated in Figure 9; symbols are at the same $x/\delta_i$ location as in Figure 9.*

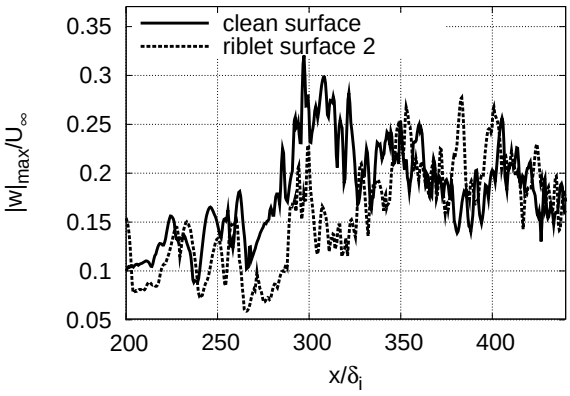


Figure 11: *Maximum spanwise velocity $|u|_{max}$ vs $x/\delta_i$.*

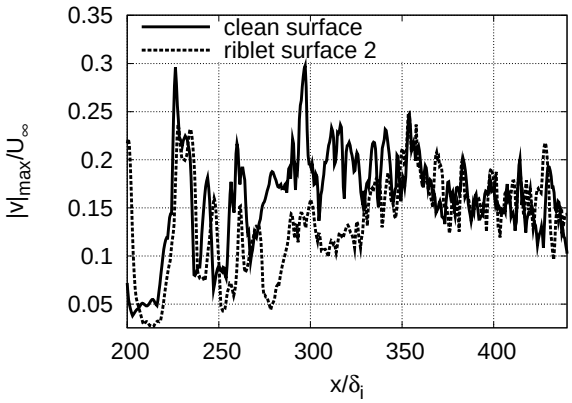


Figure 12: *Maximum wall-normal velocity $|v|_{max}$ vs $x/\delta_i$.*

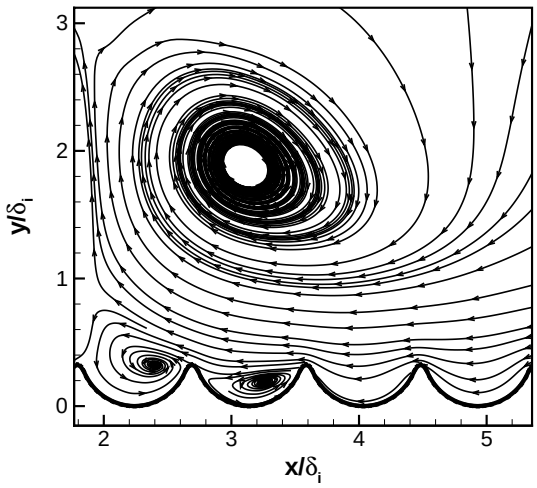


Figure 13: *Streamlines on riblet surface 2 at $x/\delta_i = 190$.*